hypothesis that a simple physical process, mediated by the trade winds, controls the broad pattern of biological productivity over the eastern equatorial Pacific on the glacial to interglacial timescale. The results do not support this hypothesis. Rather, changing upper-ocean chemistry and circulation appear to have a dominant role and need to be incorporated in a complete model of the EEP. □

Methods

Productivity estimates for calibration with the benthic foraminiferal surface sediment taxon abundance data were developed independently for the Atlantic, Pacific and Indian oceans[8,11,27,28]. Relative differences and trends in productivity among our benthic sampling locations are primarily based on CZCS (Coastal Zone Color Scanner) contours. Absolute productivity values have been selected to conform with published syntheses of measured productivity, sediment trap organic carbon fluxes, benthic chamber flux data and, where other data are lacking, the Berger[29] 'synthetic map' based primarily on oceanic phosphate concentrations. In most cases for our sample set the various sources are within 20% of the Berger[29] synthesis of measured productivity values. Recent satellite-derived estimates of surface ocean productivity (for example, ref. 30) tend to have higher absolute values than those in the previous literature. Satellite mapping is still developing, but this could mean that ultimately the values to which we have calibrated will need to be adjusted upwards. However, the trends and relative changes in productivity we used follow CZCS imagery and are compatible with satellite observations. Within the context of the calibration used here, estimation error is about 10% of the calculated value[28].

An average of 346 individuals was counted for each downcore sample and the abundances of 33 taxa were used to make palaeoestimations. Counts for the four cores were made independently by three researchers (P. L., M. Fariduddin, Q. Hui) trained in the taxonomic system used to calibrate the transfer function. Tests for no-analogue conditions, following ref. 12, show that the downcore assemblages can be modelled in terms of surface calibration data.

Received 10 September 1999; accepted 25 May 2000.

1. Barber, R. & Chavez, R. Regulation of primary productivity rate in the equatorial Pacific. *Limnol. Oceanogr.* **36,** 1803–1815 (1991).
2. Tans, P., Fung, I. & Takahashi, T. Observational constraints on the global atmosphere CO_2 budget. *Science* **247,** 1431–1438 (1990).
3. Murray, J., Barber, R., Roman, M., Bacon, M. & Feely, R. Physical and biological controls on the carbon cycling in the equatorial Pacific. *Science* **266,** 58–65 (1994).
4. Toggweiler, J., Dixon, D. & Broecker, W. The Peru upwelling and the ventilation of the South Pacific thermocline. *J. Geophys. Res.* **96,** 20467–20497 (1991).
5. Pisias, N., Mix, A. & Zahn, R. Non-linear response in the global climate system: evidence from benthic oxygen isotope record in core RC13-110. *Paleoceanography* **5,** 147–160 (1990).
6. Mix, A. & Shackleton, N. Benthic foraminiferal stable isotope stratigraphy of site 846: 0-1.8 M.A. *Proc. ODP Sci. Res.* **138,** 839–854 (1995).
7. Ninkovitch, D. & Shackleton, N. Distribution, stratigraphic position and age of ash layer 'L' in the Panama Basin region. *Earth Planet. Sci. Lett.* **27,** 20–34 (1975).
8. Loubere, P. & Fariduddin, M. Quantitative estimation of global patterns of surface ocean biological productivity and its seasonal variation on timescales from centuries to millennia. *Glob. Biogeochem. Cycles* **13,** 115–133 (1999).
9. Lampitt, R. & Antia, A. Particle flux in the deep seas: regional characteristics and temporal variability. *Deep Sea Res.* **44,** 1377–1403 (1997).
10. Loubere, P. The surface ocean productivity and bottom water oxygen signals in deep water benthic foraminiferal assemblages. *Mar. Micropaleontol.* **28,** 247–262 (1996).
11. Fariduddin, M. & Loubere, P. The surface ocean productivity response of deeper water benthic foraminifera in the Atlantic Ocean. *Mar. Micropaleontol.* **32,** 289–310 (1997).
12. Loubere, P. A multiproxy reconstruction of biological productivity and oceanography in the eastern equatorial Pacific for the past 30,000 years. *Mar. Micropaleontol.* **37,** 173–198 (1999).
13. Lyle, M. *et al.* The record of Late Pleistocene biogenic sedimentation in the eastern tropical Pacific Ocean. *Paleoceanography.* **3,** 39–59 (1988).
14. Pisias, N. & Mix, A. Spatial and temporal oceanographic variability of the eastern equatorial Pacific during the late Pleistocene: evidence from radiolarian microfossils. *Paleoceanography* **12,** 381–394 (1997).
15. Martin, J. Glacial-interglacial CO_2 change: the iron hypothesis. *Paleoceanography* **5,** 1–13 (1990).
16. Kutzbach, J. *et al.* Climate and biome simulations for the past 21,000 years. *Quat. Sci. Rev.* **17,** 473–506 (1998).
17. Rea, D. The paleoclimatic record provided by aeolian deposition in the deep sea: the geologic history of wind. *Rev. Geophys.* **32,** 159–195 (1994).
18. Mix, A. & Morey, A. in *The South Atlantic: Present and Past Circulation* (eds Wefer, G. *et al.*) 503–525 (Springer, Berlin, 1996).
19. Liu, Z. *et al.* Dynamic and observational constraints on the tropical Pacific Ocean at the last glacial maximum. *Geophys. Res. Lett.* **27,** 105–108 (2000).
20. Francois, R. *et al.* Contribution of Southern Ocean surface water stratification to low atmospheric CO_2 concentrations during the last glacial period. *Nature* **389,** 929–935 (1997).
21. Toggweiler, J. & Carson, S. in *Upwelling in the Ocean: Modern Processes and Ancient Records* (eds Summerhayes, C. *et al.*) 337–359 (Wiley and Sons, New York, 1995).
22. Barber, R. *et al.* Primary productivity and its regulation in the equatorial Pacific during and following the 1991–1992 El Nino. *Deep Sea Res. II* **43,** 933–969 (1996).
23. Fitzwater, S., Coale, K., Gordon, R., Johnson, K. & Ondrusek, M. Iron deficiency and phytoplankton growth in the equatorial Pacific. *Deep Sea Res. II* **43,** 995–1015 (1996).
24. Farrell, J., Pedersen, T., Calvert, S. & Nielsen, B. Glacial-interglacial changes in nutrient utilization in the equatorial Pacific Ocean. *Nature* **377,** 514–517 (1995).
25. Dugdale, R. & Wilkerson, F. Silicate regulation of new production in the equatorial Pacific upwelling. *Nature* **391,** 270–273 (1998).
26. Berger, W. & Lange, C. Silica depletion in the thermocline of the glacial North Pacific: corollaries and implications. *Deep Sea Res. II* **45,** 1885–1904 (1998).
27. Loubere, P. Quantitative estimation of surface ocean productivity and bottom water oxygen concentration using benthic foraminifera. *Paleoceanography* **9,** 723–737 (1994).
28. Loubere, P. The impact of seasonality on the benthos as reflected in the assemblages of deep-sea foraminifera. *Deep Sea Res. I* **45,** 409–432 (1998).
29. Berger, W. in *Productivity of the Ocean: Present and Past* (eds Berger, W., Smetacek, V. & Wefer, G.) 429–455 (Wiley, New York, 1989).
30. Antoine, D., Jean-Michel, A. & Morel, A. Oceanic primary production. 2. Estimation at global scale from satellite (coastal zone color scanner) chlorophyll. *Glob. Biogeochem. Cycles* **10,** 57–69 (1996).

Acknowledgements

We thank M. Fariduddin and Q. Hui for helping to generate the benthic count data. This work was supported by the NSF.

Correspondence and requests for materials should be addressed to P.L. (e-mail: paul@geol.niu.edu).

Annual modulation of triggered seismicity following the 1992 Landers earthquake in California

Stephen S. Gao*†, Paul G. Silver*, Alan T. Linde* & I. Selwyn Sacks*

* *Department of Terrestrial Magnetism, Carnegie Institution of Washington, 5241 Broad Branch Road, NW, Washington DC 20015, USA*

The mechanism responsible for the triggering of earthquakes remains one of the least-understood aspects of the earthquake process. The magnitude-7.3 Landers, California earthquake of 28 June 1992 was followed for several weeks by triggered seismic activity over a large area, encompassing much of the western United States[1]. Here we show that this triggered seismicity marked the beginning of a five-year trend, consisting of an elevated microearthquake rate that was modulated by an annual cycle, decaying with time. The annual cycle is mainly associated with several hydrothermal or volcanic regions where short-term triggering was also observed. These data indicate that the Landers earthquake produced long-term physical changes in these areas, and that an environmental source of stress—plausibly barometric pressure—might be responsible for the annual variation.

For this study, we used the CNSS (Council of the National Seismic System) earthquake catalogue for the period 1 January 1988 to 1 January 1997, with the aftershocks removed by declustering[2] (Fig. 1). Figure 2a shows the resulting time series of seismicity rate r (number of events per day). Before the Landers earthquake, r is relatively stable, averaging 39.7 events per day. Just afterwards, there is a sharp peak in r due to remotely triggered seismicity from the Landers event, which has been extensively studied[1,3–10]. This is followed by a remarkable annual periodicity that appears to modulate the slow decay of a post-Landers boost in seismicity (Fig. 2). The mean peak-to-peak amplitude of the annual cycle, averaged over the 4-year period 1 January 1993 to 1 January 1997 is about 10 events per day (Fig. 3). If modelled as a decaying sinusoid of the form

$$r(t) = a_1 + e^{-a_2 t}[a_3 + a_4 \sin(2\pi t - a_5)] \quad (1)$$

where t is time in years since the beginning of 1993, a decay constant of about 2 years is obtained (Fig. 2b). We tested the significance of the annual cycle by fitting the post-Landers data using equation (1), and found that a_4 is significantly different from zero at the 95% level

† Present address: Department of Geology, Kansas State University, Manhattan, Kansas 66506, USA.

for cut-off magnitudes of 1.5 and lower (Fig. 2d). The excess seismicity and its decay could not be the result of incomplete removal of aftershocks of major earthquakes such as the Landers, Big Bear, Joshua Tree and Little Skull Mountain earthquakes, because these features still exist when these aftershock zones are excluded.

The annual periodicity in seismicity is spatially localized by calculating the numbers of events N_{e1} and N_{e2} that occurred in the first half (months 1–6) and second half (months 7–12) of the years, respectively, for both the pre- and post-Landers periods. Based on Fig. 3, the difference $\Delta N_e = N_{e2} - N_{e1}$ should be highest for the post-Landers period in areas that possess a large annual cycle with a peak in the autumn. In Fig. 4, we have mapped ΔN_e for the post-Landers period. It is clear that the largest contribution comes from three areas: Long Valley, Coso and The Geysers geothermal field. These are all hydrothermal/volcanic areas and were subject to the most intense short-term triggering from Landers. This suggests a close link between the short-term triggering and the long-term seismicity. All together these three areas contribute about 2/3 of the total amplitude of the annual cycle (Fig. 3).

The variations in seismicity are detected only below magnitude 1.5 (Fig. 2d). Because for most areas, the completeness magnitude M_c (the magnitude above which no events are missed) is thought to be in the range 1.1–2.5, the catalogue is incomplete for most of the areas. It is thus necessary to determine whether the observed annual cycle could be an artefact of temporal variations in network sensitivity after the Landers earthquake compared to the preceding period. This would require the existence of an annual cycle in network sensitivity with the maximum in the autumn and minimum in the spring. A particularly sensitive measurement of network sensitivity is the seasonal variation in the number of stations that detect events at fixed magnitude. Figure 5 suggests that in the pre-Landers period, for the entire area, there are (on average) one or two more stations per event in the second half of the years than in the first half. If this made a noticeable difference in observed seismicity rate, we would expect to see an annual cycle during the pre-Landers period with peaks in the autumn. This is not the case (Figs 2b, 3). For the post-Landers period, there are several more stations per event in the first half of the years than in the second half. Again, if this made a noticeable difference in seismicity rate, we would expect to see an annual cycle with more events in the first half of the years, which is the opposite of what we have observed.

To study local variations of network sensitivity, we first divided the area into equal-sized blocks; then, for each block, we computed the number of stations per event N_{s1}, N_{s2} for the first half and second half of the years, respectively, and took the difference $\Delta N_s = N_{s2} - N_{s1}$. The spatial distribution of the resulting ΔN_s suggests that there is a great amount of spatial variability in ΔN_s. If the temporal variations in seismicity were due to variations in network sensitivity, the maps of ΔN_s and ΔN_e (Fig. 4) should be very similar. In fact, the two patterns are essentially uncorrelated. One area where ΔN_s is positive for small-magnitude events (below $M = 1.5$) is in the Long Valley area. In the vicinity of the caldera, ΔN_s varies between 1 and 2 (out of 10–20 total stations), as might be expected due to heavy snow in the winter. A detailed analysis of the seismicity of this particular zone, however, shows that the post-Landers seismicity that shows an annual cycle is primarily in the region directly south of the caldera, where ΔN_s is effectively zero. In

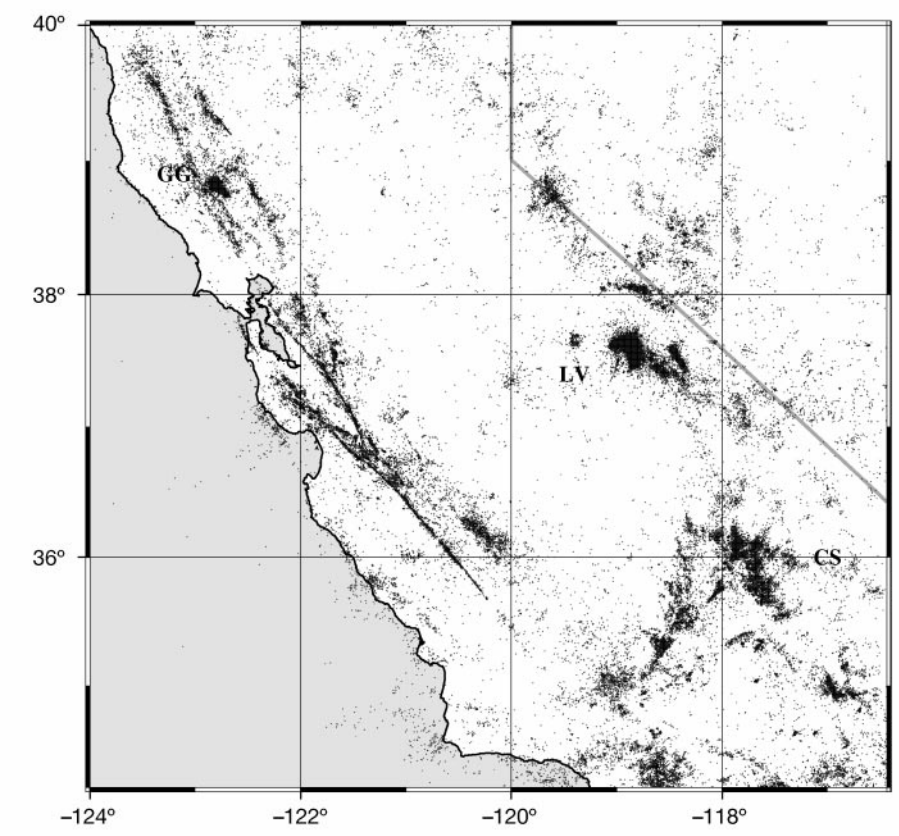

Figure 1 Map showing declustered seismicity in the western United States for the period 1 January 1988 to 1 January 1997. The total number of events in the area is about 141,000. We use a cluster-link procedure for the declustering[2]. The dimensionless scaling factor $Q = 10$ is used in the study, although our tests show that the presence of the annual cycle is insensitive to the particular value of Q used (values between 2 and 20 were used). GG, The Geysers geothermal area; LV, Long Valley; and CS, Coso. The 1992 Landers mainshock is located at the lower-right corner of the plot.

addition, considering together this zone plus the other areas with a large annual cycle, the average ΔN_s below $M = 1.5$ is very small (a few tenths of a station) and the values for the pre- and post-Landers periods are statistically indistinguishable (Fig. 5). These regions taken together nevertheless continue to reveal a clear annual cycle. Finally, this seismicity is dominated by the occurrence of swarms. It is thus highly unlikely that subtle temporal variations in network sensitivity could be the cause. The possibility that the annual cycle was the result of seasonal variation in water pumping/injection after June 1992 can also be ruled out (E. Johnson, M. Khan and S. Hodgson, personal communications).

We find that most of the swarms in this area and in the other hydrothermal/volcanic areas occurred more often in the autumn. It is this preference in the occurrence time of swarms that gives rise to much of the observed annual cycle (Fig. 2). Based on the above analysis, we conclude that variable network sensitivity is an unlikely explanation for the observed characteristics of seismicity. We propose that a real, post-Landers increase in small-event seismicity, modulated by an annual cycle, is the most likely explanation for the observed annual cycle in earthquake activity.

The data presented here reveal the existence of a long-term component of the previously observed Lander-triggered seismicity, which is modulated by an annual cycle. The excess seismicity implies a long-term change in the conditions for failure at great distance from the Landers earthquake. The predicted static stresses from the Landers earthquake are small at large distances, of the

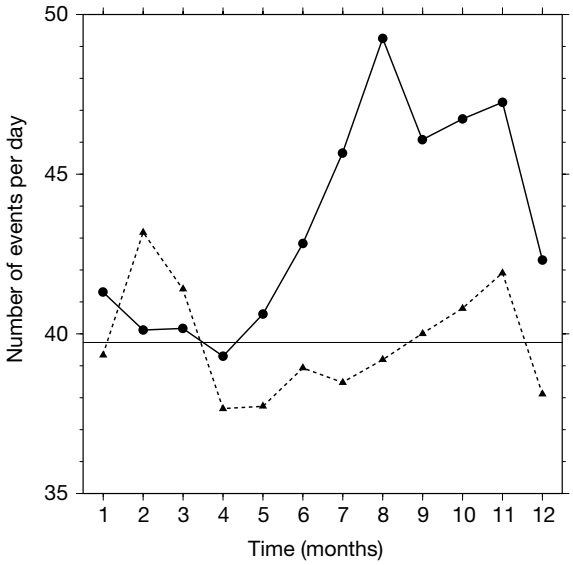

Figure 3 Average amplitude of annual modulation. Solid curve, monthly averages of seismicity-rate for the 4-year period from 1 January 1993 to 1 January 1997; dashed curve, averages for 4-year period from 1 January 1988 to January 1992. Post-Landers minimum is approximately equal to pre-Landers mean value (horizontal line).

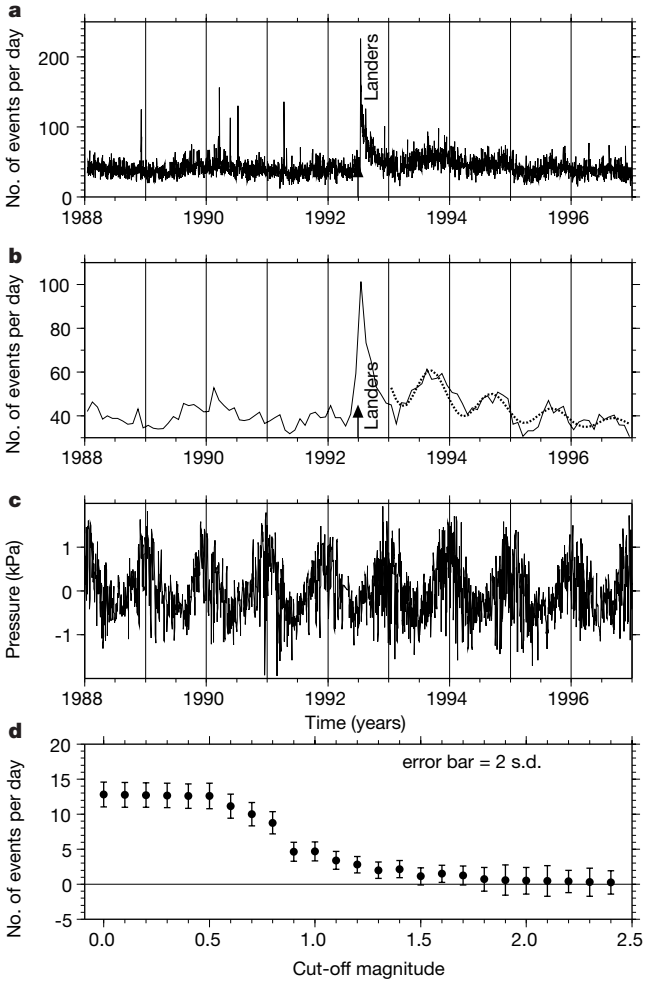

Figure 2 Time series of seismicity-rate and amplitude of the annual cycle. **a**, Number of events per day. In **b**, the solid line shows the 30-day running mean of the number of events per day, and the dotted line is the fit to equation (1). **c**, Daily mean barometric pressure recorded at a site near Long Valley. **d**, Amplitude of the annual cycle as quantified by a_4 in equation (1), calculated using different cut-off magnitudes.

order of 1 kPa (10 mbar), whereas the triggering of aftershocks appear to require a Coulomb stress that is an order of magnitude greater. The dynamic stresses (due to propagating seismic waves) from the event, however, were capable of generating 10-kPa stress changes, and this mechanism has been invoked to explain the short-term triggering[1,3,9]. If this same mechanism is responsible for the long-term triggering, it implies that dynamic stresses can produce semi-permanent changes at large distances from a seismic event.

The existence of the annual cycle requires a process that is capable of modulating the Coulomb stress for small seismic events over a large area. The most plausible sources of stress with a large annual cycle are barometric pressure and precipitation (tidal stresses at one-year period are about two orders of magnitude lower). We regard barometric pressure as the more likely of the two. This is primarily because the levels of precipitation vary dramatically throughout the regions (from large snowfall to desert environments), whereas barometric pressure fluctuations are much more coherent. Comparison of seismicity with pressure (Fig. 2) reveals that pressure lows precede seismicity highs by 90 days. Barometric pressure applies a time-varying surface load with dominant annual period and amplitude of about 2 kPa. For vertical faults, a pressure low will produce a decrease in normal stress and a corresponding increase in the effective shear stress that should produce a high in seismicity. The presence of a phase lag could be explained by the effect of fluid pore pressure on Coulomb stress. This effect is time dependent, owing to diffusion to the water table[11]. A hydrologic diffusivity of 1 $m^2 s^{-1}$—which is a high but not unreasonable value for fractured volcanic rock that characterizes the triggered regions—could produce the observed lag.

The above analysis suggests that the triggered seismicity from the Landers earthquake possesses a long-term, multi-year component. The annual periodicity is primarily observed in hydrothermal/volcanic areas. Barometric-pressure-induced modulation of seismicity may explain these data. Such a stress variation (about 2 kPa) is an order of magnitude smaller than the minimum static stress levels previously considered to trigger aftershocks[12,13]. □

Received 4 October 1999; accepted 8 June 2000.

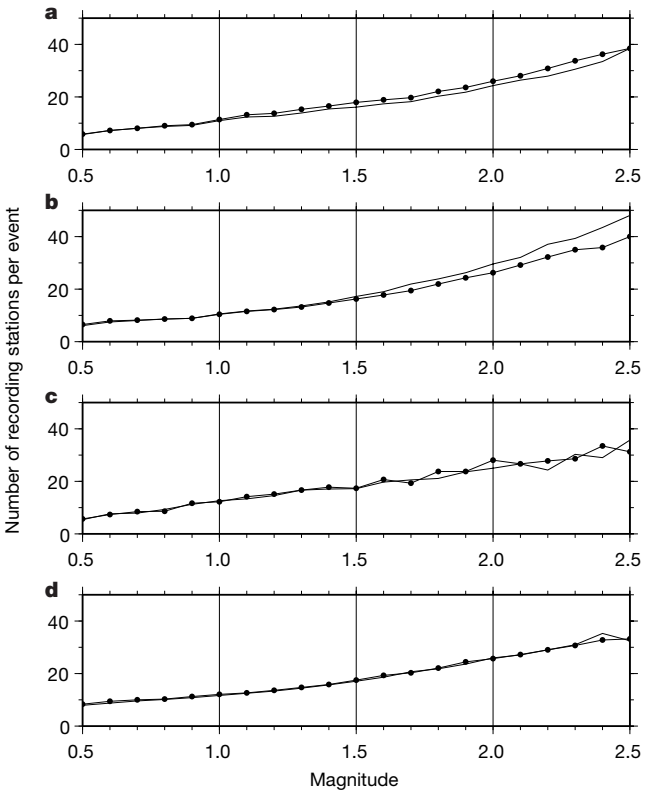

Figure 5 Number of recording stations plotted as a function of earthquake magnitude for the study area. Panels **a** and **b** show results for the entire study area. **a**, pre-Landers; **b**, post-Landers. Lines through dots are for the second half of the years, and lines without dots are for the first half of the years. Panels **c** and **d** are as **a** and **b** but for volcanic/hydrothermal regions exhibiting large annual cycles: these are the three red regions in Fig. 4, excluding northern Long Valley (see text).

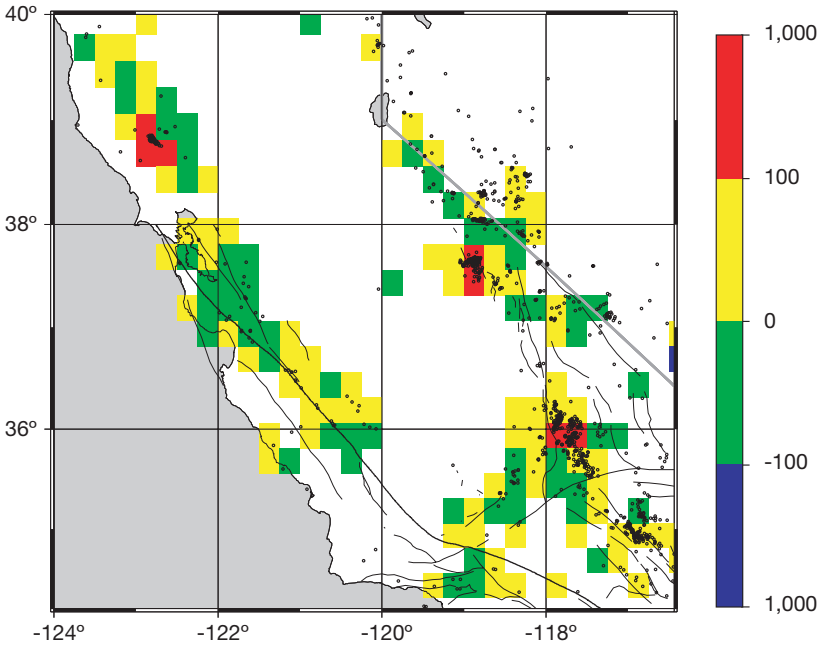

Figure 4 Map showing spatial distribution of excess seismicity in the second half of the years relative to the first half of the years for the post-Landers period. The values shown on the colour scale are the difference in the total number of events between the second half and first half of the years for the post-Landers period. Dots are events that occurred within 10 days after Landers. We note high excess seismicity in areas where short-term triggering areas was produced by the Landers earthquake.

1. Hill, D. P. *et al.* Seismicity remotely triggered by the magnitude 7.3 Landers, California, earthquake. *Science* **260,** 1617–1623 (1993).
2. Reasenberg, P. A. Second-order moment of central California seismicity 1969–1982. *J. Geophys. Res.* **90,** 5479–5495 (1985).
3. Gomberg, J. & Davis, S. Stress/strain changes and triggered seismicity at The Geysers, California. *J. Geophys. Res.* **101,** 733–749 (1996).
4. Hill, D. P., Johnston, M. J. S., Langbein, J. O. & Bilham, R. Response of Long Valley caldera to the M_w = 7.3 Landers, California, earthquake. *J. Geophys. Res.* **100,** 12985–13005 (1995).
5. Anderson, J. G. *et al.* Seismicity in the western Great Basin apparently triggered by the Landers, California, Earthquake, 28 June 1992. *Bull. Seismol. Soc. Am.* **84,** 863–891 (1994).
6. Gomberg, J. & Bodin, P. Triggering of the M_s = 5.4 Little Skull Mountain, Nevada, earthquake with dynamic strains. *Bull. Seismol. Soc. Am.* **84,** 844–853 (1994).
7. Linde, A. T. Increased pressure from rising bubbles as a mechanism for remotely triggered seismicity. *Nature* **371,** 408–410 (1994).
8. King, G. C. P., Stein, R. S. & Lin, J. Static stress changes and the triggering of earthquakes. *Bull. Seismol. Soc. Am.* **84,** 935–953 (1994).
9. Gomberg, J., Beeler, N. M., Blanpied, M. L. & Bodin, P. Earthquake triggering by transient and static deformations. *J. Geophys. Res.* **103,** 24411–24426 (1998).
10. Sturtevant, B., Kanamori, H. & Brodsky, E. E. Seismic triggering by rectified diffusion in geothermal systems. *J. Geophys. Res.* **101,** 25269–25282 (1996).
11. Roeloffs, E. in *Advances in Geophysics* Vol. 37 (ed. Dmowska, R.) 135–195 (Academic, San Diego, California, 1996).
12. Stein, R. S. & Lisowski, M. The 1979 Homestead Valley earthquake sequence, California; control of aftershocks and postseismic deformation. *J. Geophys. Res.* **88,** 6477–6490 (1983).
13. Reasenberg, P. A. & Simpson, R. W. Response of regional seismicity to the static stress change produced by the Loma Prieta earthquake. *Science* **255,** 1686–1690 (1992).

Acknowledgements

The earthquake catalogue was obtained from the Northern California Data Center maintained by UC Berkeley and the USGS. The code for declustering catalogues was written by P. Reasenberg. We thank the National Climatic Data Center and E. Roeloffs and E. Quilty for providing precipitation data; E. Roeloffs, D. Oppenheimer, S. Solomon, L. Knopoff, F. Press and H. Liu for discussions; and J. Gomberg for comments that significantly improved the manuscript.

Correspondence and requests for materials should be addressed to S.S.G. (e-mail: sgao@ksu.edu).

Ocean circulation off east Antarctica affects ecosystem structure and sea-ice extent

Stephen Nicol*, Tim Pauly*, Nathan L. Bindoff†, Simon Wright*, Deborah Thiele‡, Graham W. Hosie*, Peter G. Strutton§‖ & Eric Woehler*

* *Australian Antarctic Division, Department of the Environment and Heritage, Channel Highway, Kingston, Tasmania 7050, Australia*
† *Antarctic Co-operative Research Centre, University of Tasmania, GPO Box 252C-80 Hobart, Tasmania 7001, Australia*
‡ *School of Ecology and Environment, PO Box 423, Warrnambool, Victoria 3280, Australia*
§ *School of Biology, Flinders University of South Australia, Adelaide, South Australia 5001, Australia*

Sea ice and oceanic boundaries have a dominant effect in structuring Antarctic marine ecosystems. Satellite imagery and historical data have identified the southern boundary of the Antarctic Circumpolar Current[1] as a site of enhanced biological productivity[2]. Meso-scale surveys off the Antarctic peninsula have related the abundances of Antarctic krill (*Euphausia superba*) and salps (*Salpa thompsoni*) to inter-annual variations in sea-ice extent[3]. Here we have examined the ecosystem structure and oceanography spanning 3,500 km of the east Antarctic coastline, linking the scales of local surveys and global observations. Between 80° and 150° E there is a threefold variation in the extent of annual sea-ice cover, enabling us to examine the regional effects of sea ice and ocean circulation on biological productivity. Phytoplankton, primary productivity, Antarctic krill, whales and seabirds were concentrated where winter sea-ice extent is maximal, whereas salps were located where the sea-ice extent is minimal. We found enhanced biological activity south of the southern boundary of the Antarctic Circumpolar Current rather than in association with it[2]. We propose that along this coastline ocean circulation determines both the sea-ice conditions and the level of biological productivity at all trophic levels.

The BROKE (baseline research on oceanography, krill and the environment) survey was designed to obtain a quasi-synoptic description of the oceanography and ecosystems in an area of 873,000 km^2 off the coast of east Antarctica during the austral summer of 1996 (ref. 4; Fig. 1). Underway measurements included near-surface ocean currents, sea surface temperature, multi-frequency acoustics, surface water fluorescence and whale and seabird observations. On eight transects, detailed oceanographic measurements, primary productivity measurements, phytoplankton sampling and oblique 0–200-m zooplankton net tows were carried out at pre-determined stations.

Surface circulation between 80° and 150° E was characterized by a narrow westward slope current just north of the shelf break following bathymetric contours (Fig. 1). Flow was westward along the shelf, northwards near 80° E, with an eastward return forming a gyre closed at 115–120° E. Along the southern boundary of the Antarctic Circumpolar Current (SB-ACC), the flow was highly variable but primarily eastwards. Near 130° E, north of the SB-ACC, the flow was more strongly eastwards. This circulation pattern confirmed measurements from iceberg tracks[5] and sea-ice drift[6]. Sea surface temperatures were cooler in the west where the cool water flowed around the gyre and penetrated to lower latitudes (Fig. 1). The survey crossed the SB-ACC[1] on five transects, and with one exception the position of the SB-ACC was close to previous measurements, being further offshore in the west and closer to the coast in the east (Fig. 1).

Significantly more of the acoustically detected Antarctic krill biomass (63% or 3.0 million tonnes) was encountered in the west of the survey area (80–115° E; Table 1). In the east, Antarctic krill were confined to the narrow coastal band of cold (less than −1.6 °C) Antarctic Surface Water (AASW; Fig. 2). Antarctic krill biomass in the west was distributed throughout the latitudinally extensive cool surface waters south of the SB-ACC. Not many studies have examined Antarctic krill distribution in this region. The *Discovery*

Table 1 Biological measurements in the west (80–115° E) and the east (115–150° E) of the BROKE survey area

	Mean west (*n*)	Mean east (*n*)	*F*	*P*	d.f.
Krill acoustics*	34.39 (1076)	22.48 (927)	6.142	0.013	1,2001
Salps density (RMT net)†	0.72 (29)	38.8 (37)	65.247	< 0.0001	1,64
Primary productivity‡	613.4 (14)	395.36 (14)	11.28	0.002	1,26
Chlorophyll-*a*§	68.36 (29)	27.93 (31)	13.624	0.0005	1,58
Birds‖	70.85 (187)	30.73 (127)	5.561	0.019	1,312
Whales¶	0.066 (9)	0.003 (9)	6.181	0.024	1,16

Comparisons made by analysis of variance (ANOVA).
* Mean acoustic sa (m^2 per nautical square mile) for bins of 10 nautical miles.
† Density in individuals per 1,000 m^3 ($\log_{10}(x+1)$ transformed before analysis).
‡ Column productivity in mg C m^{-2} d^{-1} from CTD casts.
§ Vertically integrated chlorophyll *a* for 0–150 m in mg Chl-*a* m^{-2} from CTD casts.
‖ Number of birds observed in 10-minute intervals on the hour, standardized for effort.
¶ Mean number of cetaceans observed per transect, standardized for effort.

‖ Present address: Monterey Bay Aquarium Research Institute, 7700 Sandholdt Road, Moss Landing, California 95039, USA.